Effects of biaxial strain on the improper multiferroicity in *h*-$LuFeO_3$ films studied using the restrained thermal expansion method

Kishan Sinha,[1] Yubo Zhang,[2] Xuanyuan Jiang,[1] Hongwei Wang,[2] Xiao Wang,[3] Xiaozhe Zhang,[1,4] Philip J. Ryan,[5] Jong-Woo Kim,[5] John Bowlan,[6] Dmitry A. Yarotski,[6] Yuelin Li,[5] Anthony D. DiChiara,[5] Xuemei Cheng,[3] Xifan Wu,[2,*] and Xiaoshan Xu[1,7,†]

[1]*Department of Physics and Astronomy, University of Nebraska, Lincoln, Nebraska 68588, USA*
[2]*Department of Physics, Temple University, Philadelphia, Pennsylvania 19122, USA*
[3]*Department of Physics, Bryn Mawr College, Bryn Mawr, Pennsylvania 19010, USA*
[4]*Department of Physics, Xi'an Jiaotong University, Xi'an 710049, China*
[5]*Advanced Photon Source, Argonne National Laboratory, Argonne, Illinois 60439, USA*
[6]*Center for Integrated Nanotechnologies, Los Alamos National Laboratory, Los Alamos, New Mexico 87545, USA*
[7]*Nebraska Center for Materials and Nanoscience, University of Nebraska, Lincoln, Nebraska 68588, USA*

(Received 29 September 2016; revised manuscript received 6 February 2017; published 14 March 2017)

Elastic strain is potentially an important approach in tuning the properties of the improperly multiferroic hexagonal ferrites, the details of which, however, have been elusive due to experimental difficulties. Employing the method of restrained thermal expansion, we have studied the effect of isothermal biaxial strain in the basal plane of *h*-$LuFeO_3$ (001) films. The results indicate that a compressive biaxial strain significantly enhances the K_3 structural distortion (the order parameter of the improper ferroelectricity), and the effect is larger at higher temperatures. The compressive biaxial strain and the enhanced K_3 structural distortion together cause an increase in the electric polarization and a reduction in the canting of the weak ferromagnetic moments in *h*-$LuFeO_3$, according to our first principles calculations. These findings are important for understanding the strain effect as well as the coupling between the lattice and the improper multiferroicity in *h*-$LuFeO_3$. The experimental elucidation of the strain effect in *h*-$LuFeO_3$ films also suggests that the restrained thermal expansion can be a viable method to unravel the strain effect in many other thin film materials.

DOI: 10.1103/PhysRevB.95.094110

How to elastically strain a crystalline material? Conceptually, the simplest method is to apply high pressure (stress) [1]. Another method, called epitaxial strain, is to grow thin film materials epitaxially on substrates of different lattice constants [2,3]. Here, we employ a different method, called the restrained thermal expansion, in which the strain is generated in a film sample by heating the film with a laser pulse that cannot be absorbed by the substrate. Normally, thermal strain can be generated in a material in all crystalline dimensions in an isobaric thermal expansion. On the other hand, for a thin film on a substrate, if the film is heated and the substrate remains the same temperature, the out-of-plane dimension of the film is free to expand while the in-plane dimensions of the film can be restrained by the substrate (restrained thermal expansion) [Fig. 1(a)]. By comparing the material properties in the isobaric and restrained thermal expansions, the effect of isothermal compressive strain at a higher temperature can be obtained [Fig. 1(b)] (see Section S1 in the Supplemental Material [4]). This method may generate sizable strain which is difficult in brittle materials for the high-pressure method. It may also avoid side effects in the epitaxial-strain method introduced by the subtle atomic structures at the film/substrate interface [5].

To demonstrate the method of restrained thermal expansion, we studied the strain effect in hexagonal $LuFeO_3$ (*h*-$LuFeO_3$), a material that exhibits interesting improper ferroelectricity and weak ferromagnetism but is very difficult to strain elastically. In an improperly ferroelectric material, the ferroelectric order can be induced by a structural distortion [6], while in a weakly ferromagnetic material, the ferromagnetic order is typically caused by a structural distortion [7]. Therefore, in materials that are both improperly ferroelectric and weakly ferromagnetic, the structural distortions can play a critical role both in originating the ferroic orders and in coupling them. As a prototypical improper ferroelectric material, *h*-$LuFeO_3$ exhibits ferroelectricity below 1050 K and weak ferromagnetism below 130 K [8–10]. The ferroelectricity is induced by a structural distortion [K_3 structural distortion, see Fig. 1(c)] [10–13]. The ferromagnetic order, which is parasitic to the antiferromagnetic order, is induced by the K_3 structural distortion both in terms of the creation of the local magnetic moments by the Dzyaloshinskii-Moriya (DM) interactions [14,15] and in terms of the nonzero interlayer exchange interactions due to the reduction of symmetry [10,11,16,17]. First principles calculations predict a possible reversal of magnetization by an electric field along the *c* axis [11] and anomalously large magnetoelectric effects in the *a*-*b* plane in *h*-$LuFeO_3$ [18], both of which are mediated by the lattice.

In principle, detailed roles of the K_3 structural distortion could be studied by varying the distortion, e.g., by applying an elastic strain. Elastic strain is a promising tool for studying and tuning material properties, such as ferroelectricity, magnetism, catalysis, and transport properties [3,5,19–21], in addition to the methods such as chemical strain or altering the material structures, owing to the universal coupling between the crystal structure and electronic structures in materials [1,22]. This

*xifanwu@temple.edu
†xiaoshan.xu@unl.edu

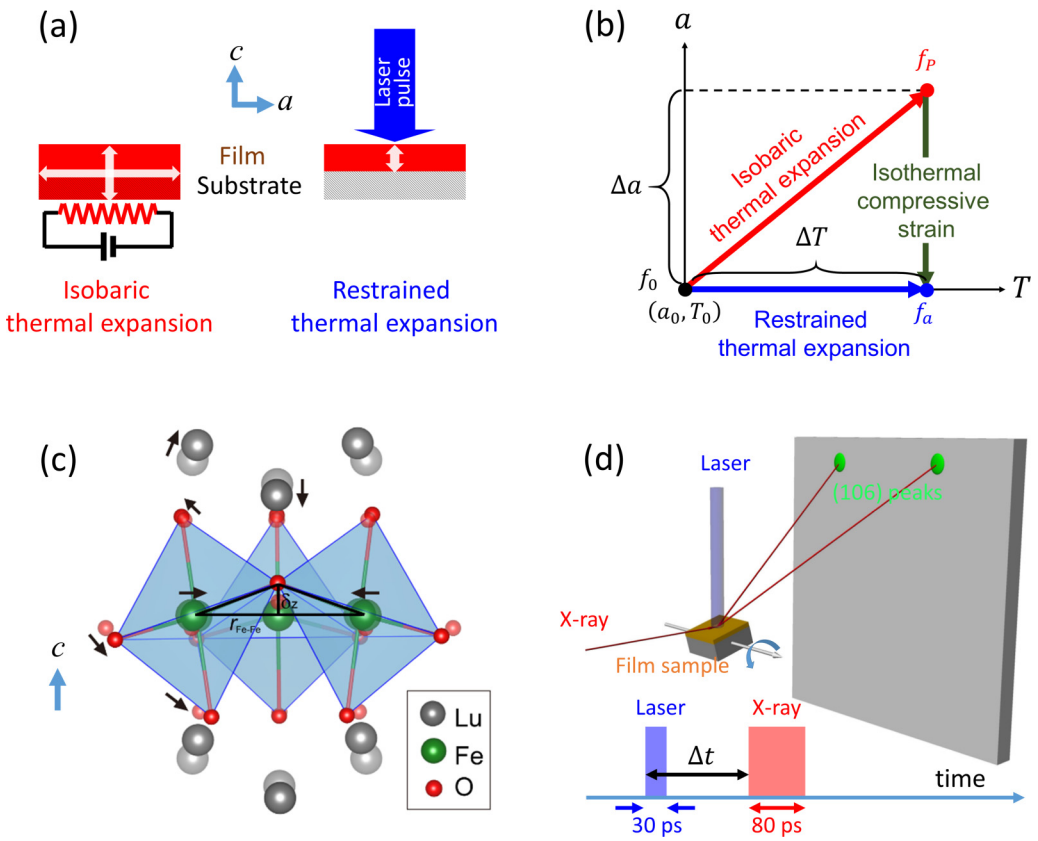

FIG. 1. (a) Schematics of the strain generated by the restrained thermal expansion in comparison with that by the isobaric thermal expansion. The arrows indicate the directions of thermal expansion. (b) Illustration of the restrained thermal expansion and isobaric thermal expansion in the (a, T) space, where a is the in-plane lattice constants, T is temperature, f is a general physical property. (c) Trimer model of the K_3 structural distortion in h-$LuFeO_3$, which corresponds to the rotation of FeO_5 trigonal bipyramids, the buckling of the Lu layers, and the trimerization. The arrows indicate the atomic displacements when K_3 is enhanced under the compressive biaxial strain. (d) Illustration of the experimental setup for the pump (laser) and probe (x-ray) measurements.

is unfortunately difficult for h-$LuFeO_3$, which is unstable in bulk but can be stabilized in epitaxial thin films: The lack of structurally compatible substrates makes the growth of defect-free films impossible and makes the epitaxial strain difficult to control [9,10,23,24], and there are no bulk counterparts to compare with since the standalone hexagonal phase of $LuFeO_3$ is unstable. As a result, investigations on the strain effect in h-$LuFeO_3$ have been rare.

Using the method of restrained thermal expansion, we studied the strain effect on the K_3 structural distortion in h-$LuFeO_3$ films. Here, the strain in the film is generated by a laser pulse; the strain and the structural distortion were measured using time-resolved x-ray diffractions. Experimentally, we observed that the compressive biaxial strain in the basal plane of h-$LuFeO_3$ significantly enhances the K_3 structural distortion, which agrees with the results of our first principles calculation. We also found from our first principles calculations that the compressive strain combined with the enhanced K_3 structural distortion increases the spontaneous electric polarizations but reduces the weak ferromagnetic moments.

Hexagonal $LuFeO_3$ (001) thin films (25 nm) were grown using pulsed laser deposition on Al_2O_3 (001) substrates [9,16,25]. In the restrained thermal expansion, the thermal strains were measured in a laser-pump x-ray-probe style [26–29], as shown in Fig. 1(d) (see Section S2 in the Supplemental Material [4]). Short durations of restrained thermal expansion in the h-$LuFeO_3$ thin film were generated using laser pulses (30 ps, 1 kHz) with the photon energy (3.2 eV) between the band gap of the Al_2O_3 substrate (8.8 eV) [30,31] and that of the h-$LuFeO_3$ film (2.0 eV) [25,32]. Time-resolved diffractions were carried out on h-$LuFeO_3$ (106) peaks to measure the lattice constants and the structural distortions, using x-ray pulses (80 ps, 12 keV), at different time delay (Δt) with respect to the laser pulses, with a two-dimensional detector. The temperature-dependent x-ray diffractions were carried out to measure the isobaric thermal expansion between 20 and 485 K at the beamline 6-ID-B, and the time-resolved x-ray diffractions were carried out at the beamline 14-ID-B of the Advanced Photon Source at the Argonne National Laboratory. Our first principles calculations are carried out based on density functional theory as implemented in the Vienna *ab initio* Simulation Package (VASP) [33]. We adopt the Perdew-Burke-Ernzerhof functional revised for solid (PBEsol) [34] where the spin-polarized generalized gradient approximation (GGA) is made in treating the exchange correlation of the electrons. A cutoff energy of 500 eV is used in the plane-wave basis with a $4\times4\times2$ k-point mesh centered at the Γ point. For transition metals, we choose $U = 4.5$ eV and

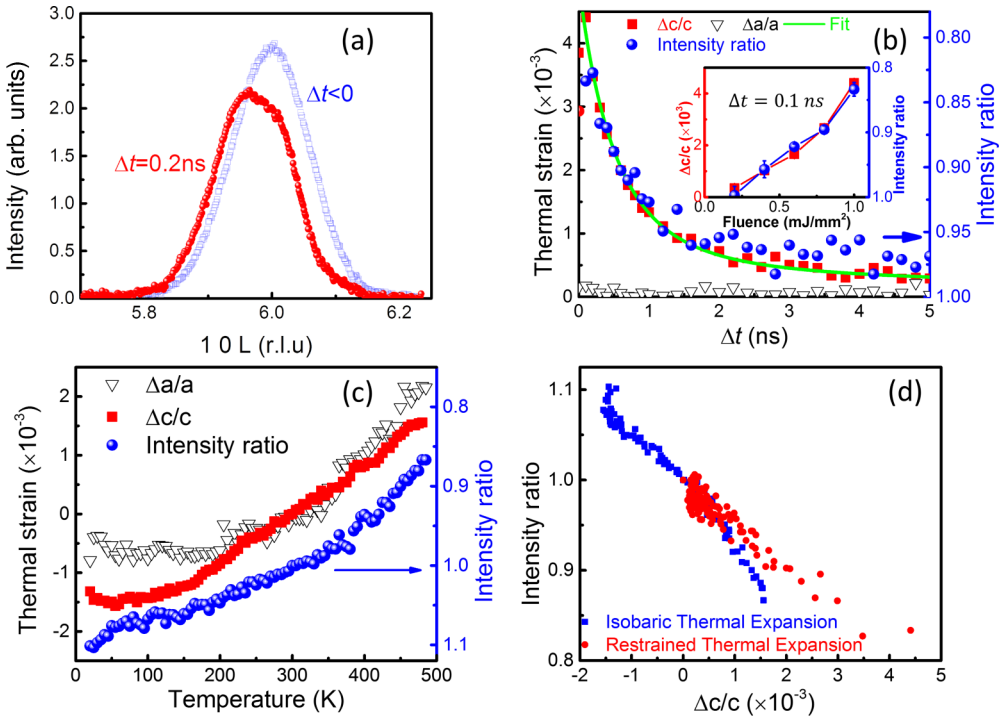

FIG. 2. Thermal strain and the intensity change of the (106) peak in the restrained and isobaric thermal expansions. (a) The diffraction profile of the (106) peak before and after the laser ($1.0\,\mathrm{mJ/mm^2}$) pulse. (b) The decay of the thermal strain $\frac{\Delta c}{c}$ and the (106) peak intensity in the restrained thermal expansion, as well as the fit using the thermal conduction model. Inset: the thermal strain $\frac{\Delta c}{c}$ and the (106) peak intensity at $t_{\mathrm{delay}} = 0.1$ ns as a function of laser fluence. (c) The thermal strain and (106) peak intensity, as a function of temperature in the isobaric thermal expansion. (d) The relation between the (106) peak intensity and the thermal strain $\frac{\Delta c}{c}$ in the restrained and isobaric thermal expansions. The (106) peak intensities are normalized using the values at room temperature.

$J_{\mathrm{H}} = 0.95\,\mathrm{eV}$. The criterion of residual Hellmann-Feynman forces for structural relaxation is $0.001\,\mathrm{eV/Å}$.

First, we demonstrate that the thermal strain only occurs in the out-of-plane direction in the restrained thermal expansion. Figure 2(a) shows the scans of the (106) peak before ($\Delta t < 0$) and after the laser pulse ($\Delta t = 0.2\,\mathrm{ns}$) of a $1.0\,\mathrm{mJ/mm^2}$ fluence. The lattice of the h-$LuFeO_3$ film at room temperature (without the laser illumination) is used as the reference coordinate system. A clear shift of the diffraction profiles in the reciprocal index L is observed in Fig. 2(a), indicating a thermal strain along the c axis. In contrast, there is no observable strain along the a axis [Fig. 2(b)], suggesting that the in-plane axis is restrained by the Al_2O_3 substrate that has no thermal strain because its band gap is too high to absorb the laser photon.

The change of the K_3 structural distortion can be estimated from the intensity change of the $(10L)$ peaks because the K_3 structural distortion is related to the diffraction intensity of $(10L)$ peaks as $I_{(10L)} \propto Q_{K3}^2$ [9] as a first-order approximation if the contribution of the oxygen is ignored (see Section S3 in the Supplemental Material [4]), where Q_{K3} is the amplitude of the K_3 structural distortion. As shown in Fig. 2(b), the (106) peak intensity decreases as the laser pulse heats the film, which is expected because the $(10L)$ peak vanishes at the ferroelectric $\rightarrow$ paraelectric transition at high temperature [9].

Next, we show that the observed time evolution of the thermal strain and the diffraction peak intensity can be explained in terms of thermal conduction. As shown in Fig. 2(b), both the change of peak intensity and the thermal strain decay over time with a similar trend. In the case of thermal conduction, the temperature in the film follows the diffusion equation $\rho c_M(\frac{\partial T}{\partial t})_z = \sigma(\frac{\partial^2 T}{\partial z^2})_t$, where ρ, c_M, T,t, z, and σ are the mass density, the mass specific heat, temperature, time, direction of the thermal conduction, and thermal conductivity, respectively [26,35]. At the film/substrate interface, the diffusion equation becomes $\rho c_M(\frac{\partial T}{\partial t})_z = g\Delta T$, where g and ΔT are the interfacial thermal conductivity and the temperature difference at the interface, respectively. The thermal strain $\frac{\Delta c}{c}$ is expected to decay in a similar trend. The only unknown parameter here is the interfacial thermal conductivity g. As shown in Fig. 2(b), we fit the time dependence of the thermal strain $\frac{\Delta c}{c}$ with the diffusion equations using g as the fitting parameter. The result shows $g = 3.8\times10^8\,\mathrm{W/(K\,m^2)}$, which falls into the proper range of the thermal conductivity of the epitaxial interfaces [36,37]. The fact that the decay of thermal strain can be explained in the light of thermal conduction suggests that temperature is a well-defined state function during the decay process (see Section S4 in the Supplemental Material [4]).

Because temperature is well defined in the decay process, one may calculate the isothermal strain effect by comparing the properties in the isobaric and restrained thermal expansions at the same temperature [Fig. 1(b)]. The thermal strain in the isobaric thermal expansion is displayed in Fig. 2(c). As the temperature increases, both a and c axes expand. The linear thermal expansion coefficients of the h-$LuFeO_3$ film around room temperature in both a and c directions are found to be $(8.0 \pm 0.1)\times10^{-6}$ (see discussion in Section S5 in the

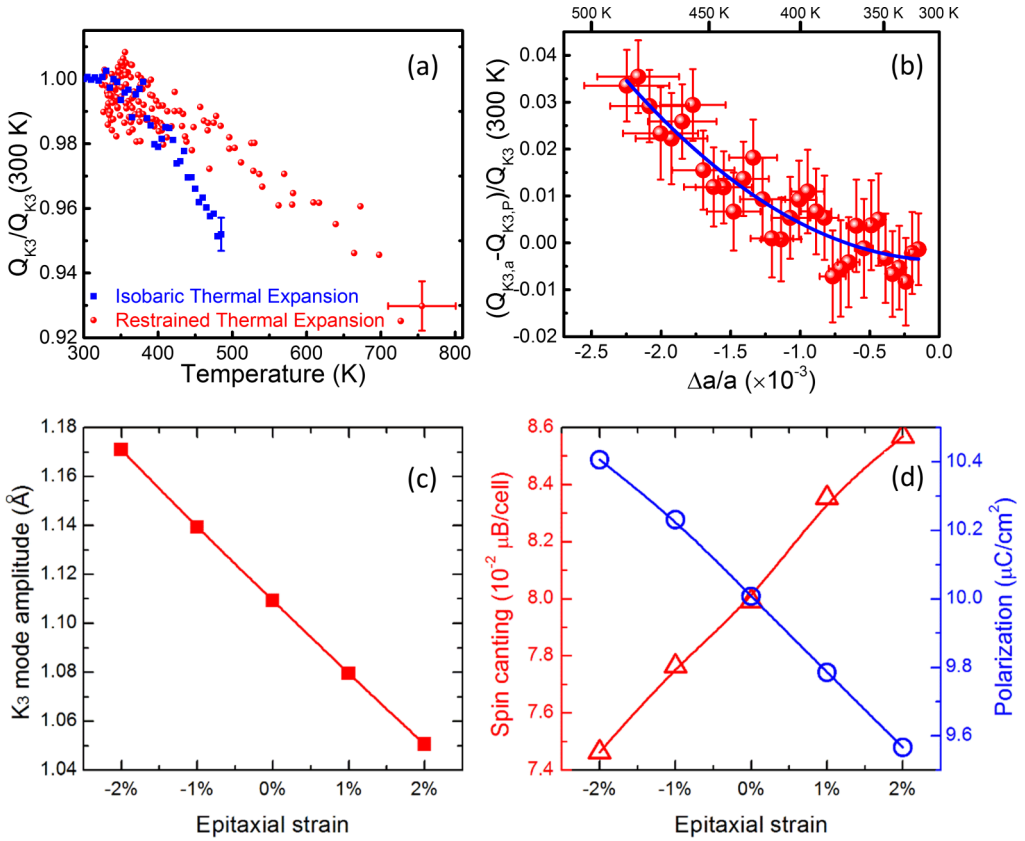

FIG. 3. (a) Temperature dependence of the amplitude of the K_3 distortion (Q_{K_3}) in both isobaric and restrained thermal expansion as a function of temperature. Representative error bars are displayed. (b) The effect of isothermal biaxial compressive strain on Q_{K_3}. Each data point represents a change of Q_{K_3} caused by a strain $\frac{\Delta a}{a}$ (bottom axis) at the corresponding temperature (top axis). The line is a guide to the eyes. (c) and (d) are the effect of the biaxial strain $\frac{\Delta a}{a}$ on the K_3 distortion and on the electric polarization and the weak ferromagnetic moment, respectively, calculated using the density functional theory.

Supplemental Material [4]). The intensity of the (106) peak also decreases as the temperature increases [Fig. 2(c)] in the isobaric thermal expansion, as it does in the restrained thermal expansion. The relation between the (106) peak intensity and the thermal strain $\frac{\Delta c}{c}$ in the restrained thermal expansion differs obviously from that of the isobaric thermal expansions, as shown in Fig. 2(d), indicating a significant strain effect.

Using the thermal and optical properties of h-$LuFeO_3$ [25,32,38], we estimated the temperature change of the h-$LuFeO_3$ film after absorbing a 1.0 mJ/mm^2 photon pulse to be ~460 K (±10%) (see Section S6 in the Supplemental Material [4]). The relation between the thermal strain $\frac{\Delta c}{c}$ and the fluence in the Fig. 2(b) inset can be converted to the relation between $\frac{\Delta c}{c}$ and temperature, which is used to estimate the temperature in the restrained thermal expansion. In Fig. 3(a), Q_{K_3} in the restrained thermal expansion, is calculated according to $I_{(10L)} \propto Q_{K_3}^2$ and the Debye-Waller factors (see Section S3 in the Supplemental Material [4] and Ref. [39]), and plotted against the temperature. Also plotted is the temperature dependence of Q_{K_3} in the isobaric thermal expansion calculated according to the data in Fig. 2(c). Obviously, Q_{K_3} is enhanced in the restrained thermal expansion.

In order to find the effect of isothermal strain on another physical property (e.g. amplitude of K_3 structural distortion Q_{K_3}), one needs to compare the temperature dependences of the physical property in the isobaric and restrained thermal expansions, as depicted in Fig. 1(b). In the restrained thermal expansion, the change of a general physical property (state function) f, relative to an initial state (a_0,T_0, f_0), can be written as $f_a - f_0 \approx (\frac{\partial f}{\partial T})_{a,\sigma_c}\Delta T$, where σ_c is the stress along the c axis. In the isobaric thermal expansion, the change of the physical properties corresponds to $f_P - f_0 \approx (\frac{\partial f}{\partial T})_{\sigma_a,\sigma_c}\Delta T$. The two processes can be related using Legendre transformation and chain rules of partial differential [35]: $(\frac{\partial f}{\partial T})_{\sigma_a,\sigma_c} = (\frac{\partial f}{\partial T})_{a,\sigma_c} + (\frac{\partial f}{\partial a})_{T,\sigma_c}(\frac{\partial a}{\partial T})_{\sigma_a,\sigma_c}$, where $(\frac{\partial f}{\partial a})_{T,\sigma_c}$ describes the isothermal strain effect, which can be found as $(\frac{\partial f}{\partial a})_{\sigma_c,T} \approx -\frac{f_a - f_P}{\Delta T}\frac{1}{(\frac{\partial a}{\partial T})_{\sigma_a,\sigma_c}}$. As shown in Fig. 1(b), if the state after the isobaric thermal expansion is used as the reference, the strain can be defined as $\frac{\Delta a}{a} \equiv -\frac{1}{a}\Delta T(\frac{\partial a}{\partial T})_{\sigma_a,\sigma_c}$ (compressive); the change of f caused by the strain is $f_a - f_P$. Figure 3(b) shows the relation between $Q_{K_3,a} - Q_{K_3,P}$ and the in-plane biaxial strain $\frac{\Delta a}{a}$. The data points indicate the strain effect at a certain temperature (top axis) measured at a certain magnitude of the strain (bottom axis). Obviously, the isothermal compressive biaxial strain enhances the K_3 lattice distortion. In addition, the effect of strain on Q_{K_3} appears to be larger at higher temperatures.

To better understand the effect of strain on the K_3 structural distortion experimentally measured by the method of restrained thermal expansion, we carried out first principles

calculations based on density functional theory to elucidate the structural distortions at the atomic level. The structures are fully relaxed, for h-$LuFeO_3$ of the space group symmetry $P_{63}cm$ under the epitaxial strains ranging from -2 to 2%. Based on the relaxed structures, the mode decompositions were performed using the group theory. The resulting Q_{K_3} are presented in Fig. 3(c) as a function of biaxial strain. Indeed, our theoretical calculations show that Q_{K_3} is enhanced (reduced) by the applied compressive (tensile) epitaxial strains, which is consistent with the experimental observation. Under the compressive strain, all the atoms are forced to be more compactly packed within the unit cell. As a result, the intralayer Fe-O bond lengths are slightly reduced, and those between Fe and apical oxygen atoms are slightly increased. In addition, the Fe-O bonds within the trimer structure also respond by a bucklering behavior compatible with the K_3 structural distortion. As schematically shown in Fig. 1(c), the oxygen atom at the center of the trimer which is shared by three bipyramids is moving up, while the other oxygen atoms in the bases of the three bipyramids are all moving downward. As a result, Q_{K_3} is increased. At the same time, the intralayer distances between two neighboring Fe or Lu atoms are reduced due to the compressive strain.

It is well known that the electric polarization is strongly coupled to the epitaxial strain in properly ferroelectric materials such as $BaTiO_3$, yet the coupling between the epitaxial strain and functional properties in multiferroic materials has been much less addressed. We next focus on the tunabilities of functional properties in h-$LuFeO_3$, including electric polarization and weak ferromagnetism, under the epitaxial strains. As an improperly multiferroic material, similar to $YMnO_3$ [13], the ferroelectric distortion in h-$LuFeO_3$ is driven improperly by the K_3 structural distortion that can be described by the rotation of FeO_5 trigonal bipyramids and the buckling of Lu layers [Fig. 1(c)], which is a highly unstable structural instability in its centrosymmetric P_{63}/mmc phase [10–13]. Therefore, it is expected that the polarization should increase as Q_{K_3} increases [12]. Indeed, as shown in Fig. 3(d), the polarization is enhanced linearly under the compressive biaxial strain. The change of polarization has a similar rate to that of Q_{K_3}. The tunability of polarization by epitaxial strain is much less than that of the conventional ferroelectric materials such as $BaTiO_3$. It indicates that the piezoelectricity is relatively small, which is consistent with a recent experiment in improper hexagonal $YMnO_3$ [40]. The weak ferromagnetism originates from both the DM interaction and single ion anisotropy. The magnitude of the DM interaction dependents on the DM vector $\mathbf{D} \sim |\mathbf{r}_{\mathrm{Fe-Fe}} \times \delta_z|$ [11,14,15], where $\mathbf{r}_{\mathrm{Fe-Fe}}$ is the displacement vector between the two iron atoms and δ_z is the displacement vector along [001] direction for the oxygen atom shared by three bipyramids in the trimer shown in Fig. 1(c), respectively. Since δ_z is closely associated with the trimerization measured by the Q_{K_3}, the weak ferromagnetism was found to be intrinsically related to the K_3 structural distortion. Therefore, an enhanced ferromagnetic moment is expected at a larger Q_{K_3} under compressive strain. However, the compressive strain also brings the two Fe atoms closer, which reduces the displacement vector $\mathbf{r}_{\mathrm{Fe-Fe}}$ more rapidly [see Fig. 1(c)]; this actually reduces amplitude of the cross product of the DM vector. As a result, the canting ferromagnetic moment is rather decreased under compressive biaxial strain [see Fig. 3(d)].

In conclusion, we have demonstrated the restrained thermal expansion method by elucidating the effect of biaxial strain on the structural distortion in improperly multiferroic h-$LuFeO_3$. We have found a significant coupling between the biaxial strain in the basal plane and the K_3 structural distortion in h-$LuFeO_3$, which in turn couples to the electric and magnetic polarizations in this improperly ferroelectric and weakly ferromagnetic material. In particular, the compressive strain enhances the K_3 structural distortion and the ferroelectric polarization, but reduces the canting of weak ferromagnetic moments. The elucidation of the strain effect in h-$LuFeO_3$ is an important advancement of our understanding on the coupling between the lattice and the improper multiferroicity. It is essential to the recently demonstrated hexagonal-ferrite superlattice structures that are promising for room-temperature multiferroicity [41], since the structural distortions in the h-$LuFeO_3$ layers are responsible for the ferroelectricity. The experimental characterization of strain effect in h-$LuFeO_3$ can potentially be extended to measure the electronic and magnetic properties, when additional probes (e.g. optical or soft x-ray) are included. This could be especially important for studying the epitaxial thin films for which the strain effects have not been fully investigated due to the imperfection in epitaxy or the lack of bulk counterparts.

The experimental effort in this paper was mainly supported by the National Science Foundation (NSF), Division of Materials Research (DMR) under Award No. DMR-1454618. X.M.C. acknowledges partial support from NSF Grant No. DMR-1053854. The theoretical effort was supported by the Air Force Office of Scientific Research under Contract No. FA9550-13-1-0124. This research used resources of the Advanced Photon Source, a U.S. Department of Energy (DOE) Office of Science User Facility operated for the DOE Office of Science by Argonne National Laboratory under Contract No. DE-AC02-06CH11357. Use of BioCARS was also supported by the National Institute of General Medical Sciences of the National Institutes of Health under Grant No. R24GM111072. The content is solely the responsibility of the authors and does not necessarily represent the official views of the National Institutes of Health (NIH). Time-resolved setup at Sector 14 was funded in part through a collaboration with Philip Anfinrud (NIH/National Institute of Diabetes and Digestive and Kidney Diseases).

[1] M. Hanfland, K. Syassen, N. E. Christensen, and D. L. Novikov, Nature **408**, 174 (2000).

[2] D. G. Schlom, L.-Q. Chen, C. J. Fennie, V. Gopalan, D. A. Muller, X. Pan, R. Ramesh, and R. Uecker, MRS Bull. **39**, 118 (2014).

[3] D. G. Schlom, L.-Q. Chen, C.-B. Eom, K. M. Rabe, S. K. Streiffer, and J.-M. Triscone, Annu. Rev. Mater. Res **37**, 589 (2007).

[4] See Supplemental Material at http://link.aps.org/supplemental/10.1103/PhysRevB.95.094110 for more details in the

experimental method, data analysis and the discussion of the thermodynamic processes.

[5] H. Wang, J. Wen, D. J. Miller, Q. Zhou, M. Chen, H. N. Lee, K. M. Rabe, and X. Wu, Phys. Rev. X **6**, 011027 (2016).

[6] A. P. Levanyuk and D. G. Sannikov, Sov. Phys. Usp. **17**, 199 (1974).

[7] R. L. White, J. Appl. Phys. **40**, 1061 (1969).

[8] Y. K. Jeong, J. Lee, S. Ahn, S.-W. Song, H. M. Jang, H. Choi, and J. F. Scott, J. Am. Chem. Soc. **134**, 1450 (2012).

[9] W. Wang, J. Zhao, W. Wang, Z. Gai, N. Balke, M. Chi, H. N. Lee, W. Tian, L. Zhu, X. Cheng, D. J. Keavney, J. Yi, T. Z. Ward, P. C. Snijders, H. M. Christen, W. Wu, J. Shen, and X. Xu, Phys. Rev. Lett. **110**, 237601 (2013).

[10] X. Xu and W. Wang, Mod. Phys. Lett. B **28**, 1430008 (2014).

[11] H. Das, A. L. Wysocki, Y. Geng, W. Wu, and C. J. Fennie, Nat. Commun. **5**, 2998 (2014).

[12] C. Xu, Y. Yang, S. Wang, W. Duan, B. Gu, and L. Bellaiche, Phys. Rev. B **89**, 205122 (2014).

[13] C. J. Fennie and K. M. Rabe, Phys. Rev. B **72**, 100103 (2005).

[14] I. Dzyaloshinsky, J. Phys. Chem. Solids **4**, 241 (1958).

[15] T. Moriya, Phys. Rev. **120**, 91 (1960).

[16] S. Cao, X. Zhang, T. R. Paudel, K. Sinha, X. Wang, X. Jiang, W. Wang, S. Brutsche, J. Wang, P. J. Ryan, J.-W. Kim, X. Cheng, E. Y. Tsymbal, P. A. Dowben, and X. Xu, J. Phys.: Condens. Matter **28**, 156001 (2016).

[17] H. Wang, I. V. Solovyev, W. Wang, X. Wang, P. J. Ryan, D. J. Keavney, J.-W. Kim, T. Z. Ward, L. Zhu, J. Shen, X. M. Cheng, L. He, X. Xu, and X. Wu, Phys. Rev. B **90**, 014436 (2014).

[18] M. Ye and D. Vanderbilt, Phys. Rev. B **92**, 035107 (2015).

[19] J. Welser, J. L. Hoyt, and J. F. Gibbons, IEEE Electron Device Lett. **15**, 100 (1994).

[20] S. W. Bedell, A. Khakifirooz, and D. K. Sadana, MRS Bull. **39**, 131 (2014).

[21] B. Yildiz, MRS Bull. **39**, 147 (2014).

[22] D. Yu, J. Feng, and J. Hone, MRS Bull. **39**, 157 (2014).

[23] E. Magome, C. Moriyoshi, Y. Kuroiwa, A. Masuno, and H. Inoue, Jpn. J. Appl. Phys. **49**, 09ME06 (2010).

[24] J. A. Moyer, R. Misra, J. A. Mundy, C. M. Brooks, J. T. Heron, D. A. Muller, D. G. Schlom, and P. Schiffer, APL Mater. **2**, 12106 (2014).

[25] W. Wang, H. Wang, X. Xu, L. Zhu, L. He, E. Wills, X. Cheng, D. J. Keavney, J. Shen, X. Wu, and X. Xu, Appl. Phys. Lett. **101**, 241907 (2012).

[26] H. Wen, P. Chen, M. P. Cosgriff, D. A. Walko, J. H. Lee, C. Adamo, R. D. Schaller, J. F. Ihlefeld, E. M. Dufresne, D. G. Schlom, P. G. Evans, J. W. Freeland, and Y. Li, Phys. Rev. Lett. **110**, 037601 (2013).

[27] D. Daranciang, M. J. Highland, H. Wen, S. M. Young, N. C. Brandt, H. Y. Hwang, M. Vattilana, M. Nicoul, F. Quirin, J. Goodfellow, T. Qi, I. Grinberg, D. M. Fritz, M. Cammarata, D. Zhu, H. T. Lemke, D. A. Walko, E. M. Dufresne, Y. Li, J. Larsson *et al.*, Phys. Rev. Lett. **108**, 087601 (2012).

[28] Y. Li, R. D. Schaller, M. Zhu, D. A. Walko, J. Kim, X. Ke, L. Miao, and Z. Q. Mao, Sci. Rep. **6**, 19302 (2016).

[29] Y. Li, C. Adamo, P. Chen, P. G. Evans, S. M. Nakhmanson, W. Parker, C. E. Rowland, R. D. Schaller, D. G. Schlom, D. A. Walko, H. Wen, and Q. Zhang, Sci. Rep. **5**, 16650 (2015).

[30] R.H. French, J. Am. Ceram. Soc. **73**, 477 (1990).

[31] E. O. Filatova and A. S. Konashuk, J. Phys. Chem. C **119**, 20755 (2015).

[32] B. S. Holinsworth, D. Mazumdar, C. M. Brooks, J. A. Mundy, H. Das, J. G. Cherian, S. A. McGill, C. J. Fennie, D. G. Schlom, and J. L. Musfeldt, Appl. Phys. Lett. **106**, 82902 (2015).

[33] G. Kresse and J. Furthmüller, Phys. Rev. B **54**, 11169 (1996).

[34] J. P. Perdew, A. Ruzsinszky, G. I. Csonka, O. A. Vydrov, G. E. Scuseria, L. A. Constantin, X. Zhou, and K. Burke, Phys. Rev. Lett. **100**, 136406 (2008).

[35] R. J. Hardy and C. Binek, *Thermodynamics and Statistical Mechanics: An Integrated Approach* (John Wiley and Sons Inc., Chichester, West Sussex, 2014).

[36] R. M. Costescu, M. A. Wall, and D. G. Cahill, Phys. Rev. B **67**, 054302 (2003).

[37] H. K. Lyeo and D. G. Cahill, Phys. Rev. B **73**, 144301 (2006).

[38] P. A. Sharma, J. S. Ahn, N. Hur, S. Park, S. B. Kim, S. Lee, J. G. Park, S. Guha, and S. W. Cheong, Phys. Rev. Lett. **93**, 177202 (2004).

[39] L.-M. Peng, G. Ren, S. L. Dudarev, and M. J. Whelan, Acta Crystallogr. Sect. A **52**, 456 (1996).

[40] Y. Geng, H. Das, A. L. Wysocki, X. Wang, S.-W. Cheong, M. Mostovoy, C. J. Fennie, and W. Wu, Nat. Mater. **13**, 163 (2014).

[41] J. A. Mundy, C. M. Brooks, M. E. Holtz, J. A. Moyer, H. Das, A. F. Rébola, J. T. Heron, J. D. Clarkson, S. M. Disseler, Z. Liu, A. Farhan, R. Held, R. Hovden, E. Padgett, Q. Mao, H. Paik, R. Misra, L. F. Kourkoutis, E. Arenholz, A. Scholl *et al.*, Nature **537**, 523 (2016).